Cell, Vol. 110, 81–91, July 12, 2002, Copyright ©2002 by Cell Press

Structural Transitions Mediating Transcription Initiation by T7 RNA Polymerase

Srabani Mukherjee, Luis G. Brieba, and Rui Sousa[1]
Department of Biochemistry
University of Texas Health Science Center
7703 Floyd Curl Drive
San Antonio, Texas 78229

Summary

During transcription initiation, RNA polymerases appear to retain promoter interactions while transcribing short RNAs that are frequently released from the complex. Upon transition to elongation, the polymerase releases promoter and forms a stable elongation complex. Little is known about the changes in polymerase conformation or polymerase:DNA interactions that occur during this process. To characterize the transitions that occur in the T7 RNA polymerase transcription complex during initiation, we prepared enzymes with Fe-BABE conjugated at 11 different positions. Addition of H_2O_2 to transcription complexes prepared with these enzymes led to nucleic acid strand scission near the conjugate. Changes in the cleavage sites revealed a series of conformational changes and rearrangements of protein:nucleic acid contacts that mediate progression through the initiation reaction.

Introduction

During transcription from +1 to +8, RNAPs appear to remain bound to promoter and frequently release short RNAs from the initial transcription complex (ITC) (Carpousis and Gralla, 1980; Hansen and McClure, 1980; Martin et al., 1988). When the RNA reaches ~9 nt, the polymerase releases the promoter and moves downstream as a stable elongation complex (EC) (Krummel and Chamberlin, 1989; Ikeda and Richardson, 1986; Straney and Crothers, 1987; Mukhopadhyay et al., 2001; Brieba and Sousa, 2001a). The stability and movement of the EC can be interrupted by certain DNA sequences, whose effects are often mediated by formation of specific RNA secondary structures (Uptain et al., 1997; MacDonald et al., 1993, 1994).

Execution of a complex reaction like transcription probably involves concerted changes in polymerase conformation and nucleic acid configuration, and some evidence for this has been obtained. For example, interactions between *E. coli* core RNAP and σ subunit cause a conformational change in the latter that unmasks its DNA binding function (Gruber et al., 2001; Kuznedelov et al., 2002), and movements of the "crab claw" features of Taq and yeast RNAPs may be induced by contact with DNA or RNA (Zhang et al., 1999; Landick, 2001; Palangat and Landick, 2001; Cramer et al., 2001; Mekler et al., 2002). Comparisons of crystal structures of T7 RNAP alone (Sousa et al., 1993, 1994), of a promoter:polymerase complex (Cheetham et al., 1999) and an ITC (Cheetham and Steitz, 1999), and of a complex with T7 lysozyme (Jeruzalmi and Steitz, 1998) reveal conformational changes in the thumb, fingers, intercalating hairpin, and C-terminal loop of the RNAP, and proteolysis experiments (Sousa et al., 1992) and steric arguments (Temiakov et al., 2000) imply a significant isomerization when the polymerase switches from initial transcription to elongation. In addition to changes in protein conformation, changes in the configuration of the nucleic acids in the transcription complex influence important steps in transcription. For example, RNA hairpin formation mediates termination at intrinsic T7 and *E. coli* RNAP terminators (MacDonald et al., 1994; Nudler, 1999; Palangat and Landick, 2001), and the ability of T7RNAP to transcribe to +8 while maintaining promoter contact appears to require that the template (T) strand "scrunch" into the polymerase (Cheetham and Steitz, 1999; Brieba and Sousa, 2001a).

Information from crystallographic studies regarding these structural transitions is, however, limited, both because the available structures provide an incomplete set of snapshots for what is likely to be a continuously dynamic process, and because it is precisely the mobile regions of a macromolecule whose conformations are sensitive to crystal packing contacts or the solution environments used for crystallization. To understand the structural changes that occur in the T7RNAP transcription complex as it progresses through initial transcription and transits to elongation, we constructed polymerases in which residues near the nucleic acid binding sites and/or on putatively mobile elements of the polymerase were mutated to cysteine. Each mutant was reacted with Fe-BABE, a reagent that conjugates to cysteines and contains a chelated Fe^{2+} (Greiner et al., 1997). Upon exposure to H_2O_2, the Fe^{2+} generates OH·, which cleave nearby nucleic acid. Cleavage positions of RNAPs carrying Fe-BABE conjugates at single sites were mapped on the T and nontemplate (NT) strands and RNA as the polymerase initiated transcription. The changes in these cleavage patterns reveal how a concerted series of conformational changes and both small- and large-scale rearrangements of protein:nucleic acid contacts mediate progression through the transcription reaction.

Results

Construction of a Cys-Minimized T7RNAP

Interpretation of Fe-BABE cleavage patterns is simplest if the protein to be conjugated has a single, accessible cysteine. Since T7RNAP has 12 cysteines, we eliminated 7 of these by consecutively mutating cysteines 530, 510, 515, 347, 723, 839, and 125 to serine (the resulting enzyme was dubbed "7−"). The remaining cysteines are buried, and mutating them reduced polymerase activity. Reactivity with DTNB corresponded to ~2 cys per native, wt RNAP (~12 cys per SDS-denatured RNAP), while reactivity of the 7− polymerase with DTNB was less than 0.2 cysteines per RNAP, indicating that the cysteines in

[1]Correspondence: sousa@biochem.uthscsa.edu

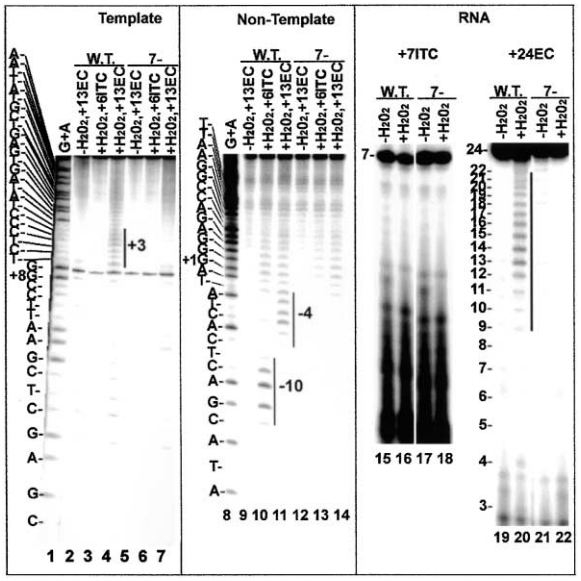

Figure 1. DNA and RNA Cleavage by Fe-BABE-Conjugated Wild-Type and Cys-Minimized (7−) Enzyme

Lanes 1–14: ECs halted at +13 (lanes 2, 4, 5, 7, 9, 11, 12, 14) or ITCs halted at +6 (lanes 3, 6, 10, 13) were formed with DNAs in which either the 5′ end of the T strand (lanes 2–7) or NT strand (lanes 9–14) was labeled with [γ-^{32}P]ATP, and with either Fe-BABE-conjugated wt (lanes 2–4, 9–11) or 7− (lanes 5–7, 12–14) enzyme. H_2O_2 was added to lanes 3, 4, 6, 7, 10, 11, 13, and 14, and cleavage was mapped by reference to G+A ladders (lanes 1, 8). Cleavage positions are highlighted by vertical bars.

Lanes 15–22: ITCs halted at +7 (lanes 15–18) or ECs halted at +24 (lanes 19–22) were formed with 3′ end-labeled RNAs and with either Fe-BABE-conjugated wt (lanes 15, 16, 19, 20) or 7− (lanes 17, 18, 21, 22) enzyme. H_2O_2 was added to lanes 16, 18, 20, and 22. Templates were a duplex T7 promoter extending from −17 to +25 in lanes 1–14, and a linearized plasmid (pPK7) containing a T7 promoter in lanes 15–22.

the 7− enzyme would be inaccessible to conjugation with Fe-BABE. To see if the 7− enzyme would provide a suitable background for examining cleavage by Fe-BABE, we compared cleavage patterns of Fe-BABE-conjugated wt and 7− enzymes (Figure 1). The wt enzyme cleaves the T strand near +3 in an EC halted at +13 (lane 4). It cleaves the NT strand in an ITC and an EC near −10 and −4, respectively (lanes 10 and 11). The wt enzyme also cleaves the 5′ region of the RNA in an EC halted at +24 (lane 20). The 7− enzyme shows little cleavage in any of these complexes, and therefore provides a suitable background in which to observe DNA or RNA cleavage by Fe-BABE conjugated to single cysteines introduced into the RNAP.

Cleavage Patterns of Fe-BABE Tethered to Introduced Cysteines

T7RNAP is organized around a large cleft that contains the active site and in which the T strand binds (Figure 2D). Surrounding this cleft are structures—the thumb (aa 330–410) and fingers (aa 540–740, 826–883) subdomains and intercalating hairpin (aa 232–242)—that change conformation upon promoter binding (Cheetham et al., 1999). Cysteines were introduced into these elements at positions 239, 385, 388, 393, 394, and 644 where, based on the structure of an ITC with a 3 nt RNA (Cheetham and Steitz, 1999), they would be expected to cleave the RNA inside the T strand binding cleft, and/or the T and NT strands near, and downstream of, the upstream edge of the transcription bubble (Figure 2D, Downstream Conjugates). Cysteines were also introduced into the promoter recognition loop (aa 740–770) at 764 and 745 and into the N-terminal domain (aa 1–310) at 153 and 303. Conjugates at these positions (and at an endogenous cys at 723) should cleave DNA upstream of the transcription bubble and might also cleave the RNA after it emerges from the T strand binding cleft and begins to exit the EC (Figure 2D, Upstream Conjugates).

Mutant polymerases conjugated with Fe-BABE were used to cleave DNA in complexes to which NTPs allowing RNA extension to 1, 4, 6, 7, or 13 nt were added. Complexes with RNA 1–7 nt in length are denoted ITC1, ITC4, etc. (ITC1 corresponds to adding only 3′ dGTP to the reaction), and the EC with the 13 nt RNA is EC13. The ITCs are dynamic, with RNAs being continuously synthesized and released, so the observed cleavage sites could represent time- and population-averaged composites of multiple states. However, kinetic studies show that the slowest step in abortive cycling by T7RNAP is release of the transcript whose extension is halted by NTP limitation (Jia and Patel, 1997; Villemain and Sousa, 1998; Huang et al., 1999). The ITC populations should therefore be dominated by complexes with RNAs of the specified length. A conjugate is referred to by the number of the residue to which it is tethered.

Since cleavage by Fe-BABE is through diffusible OH·, cleavage diminishes with distance to target with no sharp cut-off (Han and Dervan, 1994), and interposition of protein or nucleic acid between the conjugate and the target can block cleavage. For example, cysteines 385, 388, 393, and 394 are close in space, but sit on different faces of helix N of the thumb subdomain. Residues 385 and 388 are adjacent and face away from the T strand binding cleft, while 394 faces into this cleft and 393 occupies an intermediate position (Figure 2D). If the NT strand in the ITC lies outside the T strand binding cleft, it would be most accessible to cleavage by 385/388 and inaccessible to 394. The NT strand cleavage patterns of these conjugates bear this out. NT strand cleavage in the ITCs is strongest with 385 (Figure 2A, lanes 1–4), followed by 388 (Figure 2A, lanes 6–9; reduced cleavage by 388 probably reflects both greater distance and interposition of Y385 between 388 and the NT strand). NT strand cleavage is further diminished for 393 (Figure 2A, lanes 11–14) and is undetectable for 394 (lanes 16–19).

An inverse relationship is expected for T strand cleavage, since 394 should cleave T strand inside the cleft, while 385 and 388 should not (Figure 2D). This is borne out by the T strand cleavage, at least for ITCs 1 and 4. In ITC1, 394 cleaves T strand at −4/−5 (Figure 2B, lane 16). As the RNA is extended from 1 to 7 nt, cleavage appears at more downstream positions (Figure 2B, lanes 16–19). Significantly, T strand cleavage by 394 at −4/−5 persists even as cleavage at −3 (lane 17), −1 (lane 18), and +1 (lane 19) develops in ITCs 4, 6, and 7, respectively. This suggests that the −4/−5 nts are not moving away from 394 even as more downstream DNA is moving closer, i.e., it is consistent with the idea that the T strand

is scrunching into the T strand binding cleft. On the opposite side of helix N, 385 and 388 cleave T strand weakly around −9 in ITCs 1 and 4 (Figure 2B, lanes 1, 2, 6, and 7). This is consistent with the ITC3 structure (Figure 2D), which reveals that the NT strand and intercalating hairpin protect T strand downstream of −8 from OH· generated at 385/388, while T strand upstream of −10 is protected by NT strand and the promoter recognition loop, so that only −8 to −10 of the T strand would be accessible to OH· generated at 385/388 (as suggested by the red arrow in Figure 2D). However, in ITC6, cleavage at −9 diminishes or disappears, and cleavage appears around −2 (Figure 2B, lanes 3 and 8), and then shifts to −1 in ITC7 (lanes 4 and 9).

A change in the position of cleavage by any given conjugate could reflect movement of the polymerase as a whole, reorientation of DNA within the complex, or conformational changes in the polymerase. Therefore, assignment of changes in cleavage sites to specific structural transitions relies, at least in part, on subjective considerations. In our analysis, conformational changes were identified as instances in which cleavage by a given conjugate changed in a manner distinct from that of conjugates cleaving in the same regions, while changes due to translocation or reorientation of the DNA were identified as instances in which cleavage by several conjugates changed in a concerted manner. For example, the shift in T strand cleavage by 385/388 from −9 to −2 upon RNA extension from 4 to 6 nt is unlikely to reflect T strand translocation because cleavage by upstream conjugates indicates that the −9 region of the T strand does not move during initial transcription (Figures 2F and 2G). Further, this 7 nt shift in cleavage position is much larger than the 2 nt increase in RNA length that accompanies it, and it also moves cleavage by 385/388 from outside of the T strand binding cleft (T strand −8/−9) to inside (T strand −1/−2), which is difficult to reconcile with the structure in Figure 2D. This all suggests that extension of the RNA from 4 to 6 nt causes a conformational change in the thumb, probably a bending toward the RNA, as suggested by the blue arrow in Figure 2D. This would allow OH· generated at 385/388 into the T strand binding cleft and would block OH· from reaching regions of the T strand upstream of the intercalating hairpin.

If the thumb bends upon RNA extension from 4 to 6 nt, a change in NT strand cleavage by 385/388 at this point is also expected. NT strand cleavage at −5 in ITCs 1 and 4 disappears or diminishes sharply in ITC6 (Figure 2A, lanes 1–4 and 6–9). This does not appear attributable to NT strand translocation, since NT strand cleavage by 393 (Figure 2A, lanes 11–14) or 239 (Figure 2E, lanes 1–4) hardly shifts as the RNA is extended from 1 to 7 nt. However, bending of the thumb toward the RNA would block cleavage at −5 by interposing the intercalating hairpin between 385/388 and NT strand −5 (Figure 2D). Since cleavage by 393 and 394 does not exhibit the same shifts seen with 385/388, this indicates that the "hinge" in the bending of the thumb is between 388 and 393.

Extension of RNA from 7 to 13 nt shifts T strand cleavage by 385/388 from appx. −1 to appx. +7 (Figure 2B, lanes 4, 5, 9, and 10) and shifts the strongest cleavages on the NT strand from appx. −1 to appx. +6 (Figure 2A, lanes 4, 5, 9, and 10). This probably reflects polymerase translocation, since cleavage shifts by a distance similar to the length of the RNA extension. However, cleavage by 385/388 also increases in intensity in EC13, and on the NT strand a biphasic pattern of cleavage develops with centers at appx. +6 and appx. −2. This biphasic pattern is seen with 385, 388, and 393, though with 385 the +6-centered cleavage is strongest (Figure 2A, lane 5), with 393 the −2-centered cleavage is stronger (lane 15), and 388 exhibits similar intensities for both sets cleavages (lane 10). These changes suggest that extension of the RNA from 7 to 13 nt is associated not simply with translocation of polymerase, but also with a reorganization of the transcription complex.

Residue 239 is part of the intercalating hairpin, which is important for promoter melting, and stacks between the T and NT strands on the −5 bp in ITC3 (Figure 2D). Like 394, 239 faces the T strand binding cleft but is not as deep in the cleft (Figure 2D). Like 394, 239 cleaves T strand at −4/−5 in ITC1 (Figure 2C, lane 1), and its cleavage pattern lengthens by downstream extension as the RNA extends from 1 to 7 nt (Figure 2C, lanes 1–4). However, 239 can also cleave the more downstream T strand as it emerges from the ITC (Figure 2D, +5) and displays a second set of T strand cleavages between +6 and +14 in ITCs 4 to 7 (Figure 2C, lanes 2–4; failure to detect such cleavage in ITC1 may reflect the fact that the T7RNAP open complex is not fully stabilized until RNA synthesis begins; Brieba and Sousa, 2001b). These cleavages shift as the RNA is extended from 4 to 7 nt. For example, 239 cleaves T strand between +6 and +11 in ITC4 (lane 2) and between +9 and +14 in ITC7 (lane 4). Comparable shifts are not seen for 239 NT strand cleavages, which extend from −4 to +6 in ITCs 1 through 7, though cleavage intensity varies as the RNA grows (Figure 2E, lanes 1–4).

In EC13 the biphasic pattern of T strand cleavage by 239 disappears and is replaced by a single cleavage site around −2 (Figure 2C, lane 5). Thus, while 239 in ITC7 cleaves the T strand 0–3 and 13–17 nt downstream of the upstream edge of the transcription bubble, in EC13 it cleaves 3–7 nt upstream of the bubble. It is difficult to explain the loss of T strand cleavage downstream of the upstream edge of the bubble and appearance of cleavage upstream of the bubble, if the conformation of the intercalating hairpin in EC13 is like that in ITC3 (Figure 2D). This suggests that transition to elongation involves a conformational change in the intercalating hairpin.

Residue 644 is on the edge of the fingers subdomain, which forms the side of the T strand binding cleft opposite the thumb and intercalating hairpin and binds T strand near the RNA 3′ end (Figure 2D). Changes in cleavage by 644 indicate that transition to elongation may also cause a change in the fingers subdomain conformation or interaction with DNA, since 644 cleaves the T and NT strands around +18 and +12, respectively, in EC13 (Figures 2C and 2E, lane 10) but cleaves neither strand in the ITCs (Figures 2C and 2E, lanes 6–9).

The upstream conjugates (303, 764, 745, 153, and 723) cleave DNA upstream of −5 in ITCs 1–7 (Figures 2F and 2G). The static nature of the contacts between the polymerase and the −5 to −17 element of the promoter during RNA extension from 1 to 7 nt is revealed by the

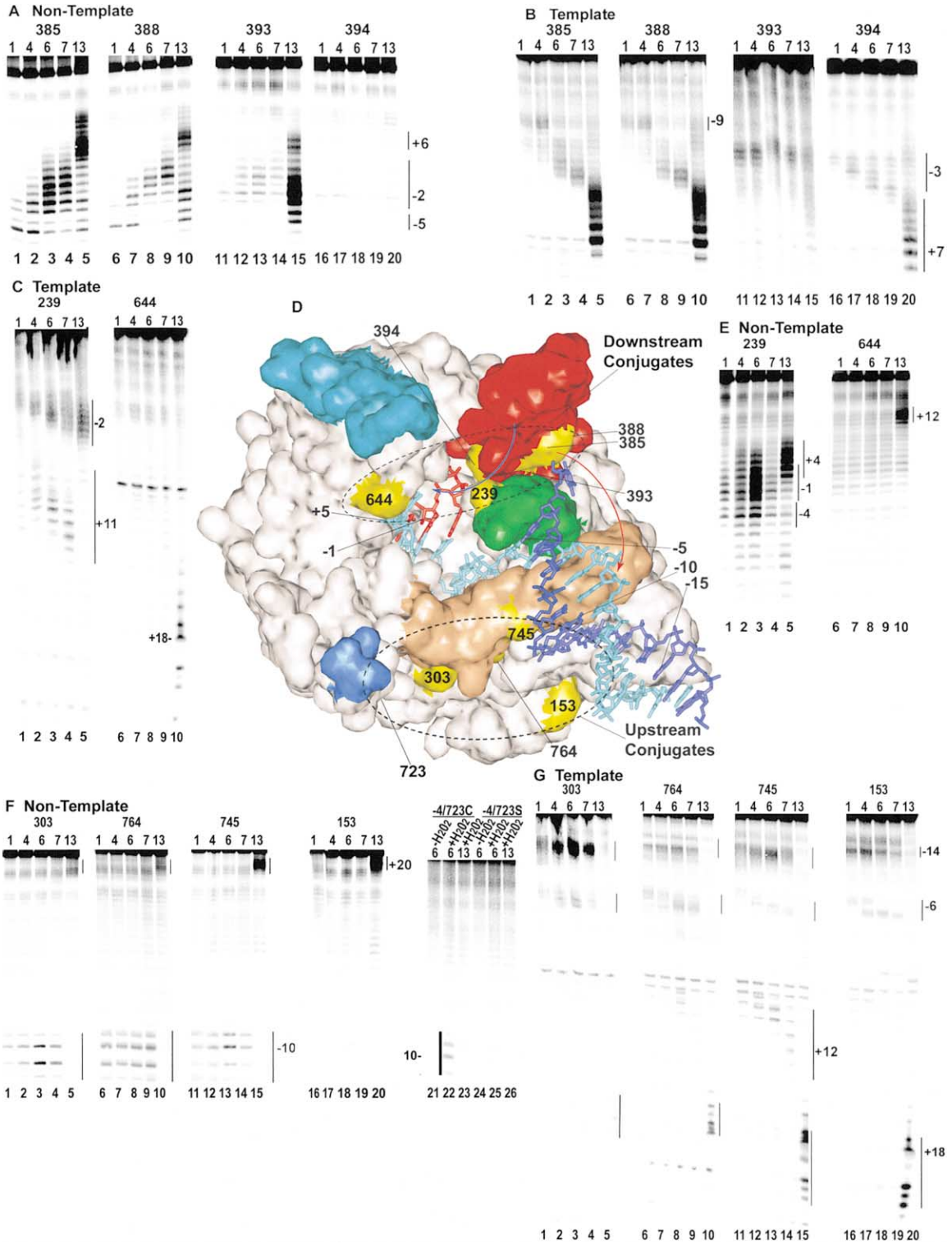

Figure 2. DNA Cleavage by Fe-BABE Tethered to Introduced Cysteines

(A) Cleavage of transcription complexes with 5′ end-labeled NT strand by conjugates at aa positions 385 (lanes 1–5), 388 (lanes 6–10), 393 (lanes 11–15), or 394 (lanes 16–20). The RNA length in the complex is 1, 4, 6, 7, or 13 nt as indicated at the top of each lane (a length of 1 corresponds to adding only 3′-dGTP).

(B) As in (A), but with 5′-labeled T strand.

(C) As in (B), but with conjugates at either 239 (lanes 1–5) or 644 (lanes 1–10).

(D) Crystal structure of a T7RNAP ITC with a 3 nt RNA (PDB # 1QLN). NT strand is dark blue; T strand is cyan; RNA is red; the promoter recognition loop is tan; the thumb subdomain (aa 330–410) is red; the intercalating hairpin (aa 232–242) is green; the fingers flap (aa 586–620) is cyan; and the positive patch (K711/713/714) is blue. Positions of Fe-BABE conjugation are yellow and are labeled (aa 723 is hidden; 764

essentially invariant pattern of cleavage of the −9 to −12 region of the NT strand in ITCs 1 to 7 (Figure 2F, lanes 1–4, 6–9, 11–14, and 22), as well as by the T strand cleavages centered at −14 and −6 (Figure 2G, lanes 1–4, 6–9, 11–14, and 16–19; a shift in the center of the −6 cleavage by 1–2 nt upon RNA extension from 1 to 6 nt may reflect stabilization of the transcription bubble). NT strand cleavage of −9 to −12, and of the flanking regions of the T strand, is consistent with how the duplex presents either T or NT strand to face the upstream conjugates (Figure 2D). OH· generated at 745 is also able to reach T strand downstream of the RNA 3′ end (Figure 2D, +5), so that 745 cleaves T strand between +8 and +14 in ITCs 4 to 7 (Figure 2G, lanes 12–14). As seen for cleavage in the same region by 239, these cleavages shift downstream as the RNA grows, indicating that this region of the T strand is moving relative to the polymerase even as contacts with more upstream DNA are immobile.

In EC13, cleavage upstream of −5 disappears (Figures 2F and 2G, lanes 5, 10, and 15), reflecting promoter release. However, if DNA upstream of the RNA were similarly positioned in EC13 and the ITCs, we would expect the upstream conjugates in EC13 to cleave somewhere between +6 and −9 (i.e., 7–22 nt upstream of the RNA 3′ end, as seen in the ITCs). However, the upstream conjugates do not cleave DNA upstream of the RNA in the EC. Instead, they cleave downstream of the RNA, near +20 in the NT strand and +18 in the T strand (Figures 2F and 2G, lanes 5, 10, and 15). It is unlikely that binding to the end of the DNA by a second polymerase can account for this cleavage because (1) the DNAs used here extend only to +25, so a polymerase halted at +13 would occlude all but 8 bp of downstream DNA from being bound by a second molecule; (2) this far downstream cleavage is seen only when NTPs allowing formation of EC13 are present; and (3) addition of heparin to block nonspecific DNA binding had no effect on cleavage patterns (not shown). Finally, we carried out similar experiments with 745 and 153 using DNAs that extend to +30. If the far downstream cleavage were due to end binding by a second molecule, use of a longer DNA would shift this cleavage further downstream, but cleavage in EC13 was centered near +19, irrespective of the length of the DNA (not shown). Thus, the far downstream cleavage in EC13 is attributable to the polymerase halted at +13. The observation that transition to elongation switches DNA cleavage by the upstream conjugates from upstream to downstream of the RNA 3′ end further indicates that this transition involves a reorganization of the transcription complex.

Discontinuous Translocation of Upstream and Downstream Regions of the T Strand upon NTP Binding

NTP binding to the ITC alters $KMnO_4$ reactivity of the T strand, suggesting that NTP binding alters T strand:RNAP interactions (Brieba and Sousa, 2001a). We therefore examined the effect of NTP binding on T strand cleavage by 239 (Figure 3A). The cleavage patterns are discussed in reference to Figure 3B, which shows a superposition of the DNA from a T7RNAP:promoter structure (Cheetham et al., 1999) and ITC3 (Cheetham and Steitz, 1999). Also shown are the RNA and the intercalating hairpin from ITC3. The −4-centered cleavage in ITC4 (Figure 3A, lane 1) is consistent with the proximity of 239 to −4 of the T strand in ITC3 (Figure 3B). Scrunching of the T strand upon extension of the RNA gives rise to the downstream extension of the −4 cleavage pattern seen in lanes 2 and 3. T strand cleavage between −1 and +5 is undetectable, perhaps reflecting the distance between 239 and the +1 to +4 region and protection by RNA (Figure 3B). However, 239 does cleave T strand downstream of +5 (Figure 3A, lane 1), reflecting how a bend brings the more downstream region of the T strand close to 239. Translocation of the T strand through the polymerase moves more downstream DNA toward 239, leading to the shifts in the downstream (+5 to +14) cleavage patterns seen in lanes 1–3. To determine how NTP binding affects translocation, we added increasing concentration of the elongating NTP to the 3′-dCMP-terminated ITC7 (lanes 3–7). Increasing [NTP] has no effect on cleavage at the upstream (−4) site. However, the center of the downstream (+11) cleavages shifts downstream as [NTP] increases (addition of incorrect NTP had no effect, and NTP binding had no effect on NT strand cleavage; not shown). A net shift of ~1 nt in lane 3 versus lane 7 is confirmed by the superimposed scans of the +8 to +14 regions of lanes 3–7 (shown to the right of the gel). Translocation of the T strand downstream of the RNA 3′ end may therefore occur when NTP binds, during which the −4 to +1 segment doesn't move. After NMP incorporation, the +1 to −4 segment must then "catch up" with the more downstream element. During this cycle of discontinuous translocation, T strand:polymerase contacts are likely to change, which may account for the NTP binding-dependent changes in T strand $KMnO_4$ reactivity.

Cleavage of RNA in the ITC and EC

Cleavage of RNA by the upstream conjugates is shown in Figure 4A (lanes 1–12) for an EC with a 24 nt RNA. Peak cleavage by 303 and 764 is at −10, though 764 cleaves slightly upstream of 303 (lanes 2 and 4; numbering refers to distance from the RNA 3′ end with the most 3′ nt numbered 0). Peak cleavage by 745 is at −8 (lane 6), while cleavage by 153 and 723 is centered at −13 (lanes 8 and 10), though 723 cleaves with reduced intensity (lane 10). Conjugate positions are indicated in Figure 4C, on a display of the surface charge distribution of the polymerase. Strikingly, a positively charged groove is identified on the upstream face of the enzyme. RNase protection, crosslinking, and $KMnO_4$ reactivity indicate

and 393 are largely obscured). Numbering of the DNA is relative to the +1 start site, and numbering of the RNA is relative to the RNA 3′ nt.
(E) As in (C), but with 5′-labeled NT strand.
(F) As in (A), but with conjugates at 303 (lanes 1–5), 764 (lanes 6–10), 745 (lanes 11–15), and 153 (lanes 16–20). Also shown is cleavage by an Fe-BABE-conjugated enzyme from which four cysteines have been removed, but which retains a cys at 723 (lanes 21–23), and an enzyme in which C723 was mutated to ser (lanes 24–26). H_2O_2 was added to all reactions except those in lanes 21 and 24.
(G) As in (F), but with 5′-labeled T strand.

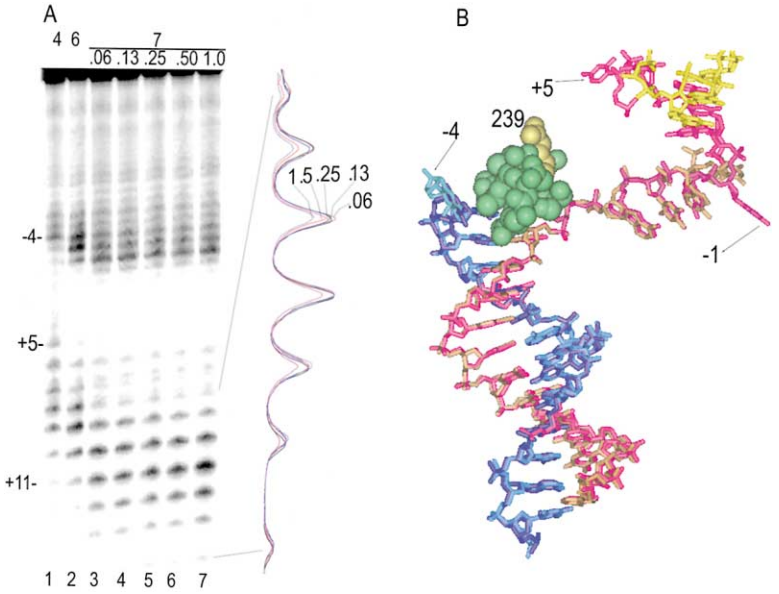

Figure 3. Effects of NTP Binding on T Strand Cleavage

(A) T strand cleavage by 239 as a function of RNA length and elongating NTP concentration. RNA length is specified above the gel lanes. In lanes 3–7, the RNA is 3′-dCMP terminated and the elongating NTP is present at 0.06 to 1.0 mM. Superimposed scans of the +8 to +14 regions of lanes 3–7 are shown to the right of the gel.

(B) Superposition of DNA and intercalating hairpin from a T7RNAP:promoter complex structure (PDB # 1CEZ) and a T7RNAP ITC structure. DNA from the promoter complex is light brown (T strand) and dark blue (NT strand). DNA from the ITC is magenta (T strand) and cyan (NT strand); RNA is yellow. The intercalating hairpin is green, except for residue 239, which is yellow.

that the RNA:DNA hybrid in a T7RNAP EC is 7–8 bp long, with ~6 nt of single-stranded RNA binding to a site located at least partly on the N-terminal domain (Temiakov et al., 2000; Huang and Sousa, 2000). The positively charged groove identified in Figure 4C lies mostly on the N-terminal domain and accommodates ~6 nt of RNA. If −8 to −13 of the RNA is modeled in this groove, with −8 at its downstream edge, then 303 and 764 lie close to −10, with 764 slightly downstream of 303. The asymmetric distribution of cleavage by 303/764 is readily understood, since downstream of −8 the RNA would pass into the large cleft of the polymerase, becoming inaccessible to OH· generated at 303/764. The 745 and 153 cleavages are also readily interpreted in term of this model. The weak cleavage by 723 is consistent with its distance from this putative RNA bind-

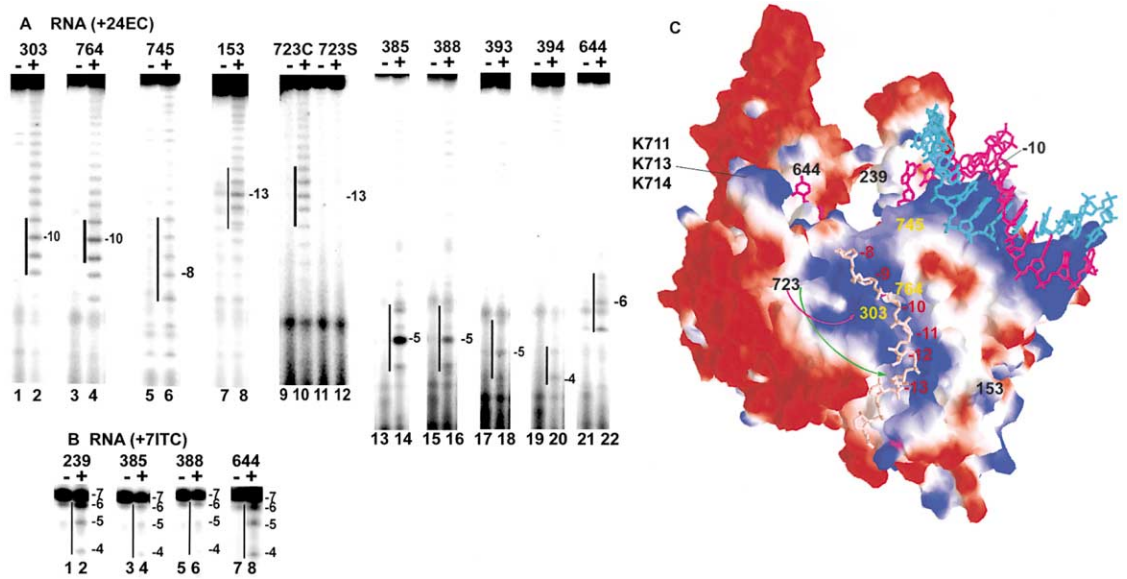

Figure 4. RNA Cleavage

(A) RNA cleavage by 303, 764, 745, 153, 723, 385, 388, 393, and 394 in ECs halted at +24. For each pair of lanes, minus sign and plus sign denote absence or addition of H_2O_2, respectively. RNA was 3′ end labeled by incorporation of a single [α-^{32}P]CMP at −1. Numbering denotes distance from the RNA 3′ end.

(B) RNA cleavage by conjugates at 239, 385, 388, and 644 in ITC7.

(C) Structure of T7RNAP ITC with surface charge potential colored blue for positive and red for negative. T strand is magenta and NT strand is light blue. The phosphate ribose backbone of an 8 nt single-strand of RNA (in light pink) is modeled into a positively charged groove on the upstream face of the polymerase. The positions of residues 153, 239, 303, 644, 745, 764, and 723 are labeled. A positively charged cluster of three lysines (K711/713/714), which may interact with downstream DNA in the EC (see Discussion), is also indicated.

ing groove, but it is not immediately apparent why 723 cleavage is strongest at −13, rather than at the closer −9/−10. However, inspection of Figure 4C reveals that, if RNA is bound in the groove, a wall of protein would partially protect −9 to −12 from OH· generated at 723 (as suggested by the magenta arrow in Figure 4C). This wall ends at the upstream edge of the groove, allowing OH· a free path from 723 to −13 (suggested by the green arrow). These data indicate that RNA from −8 to −13 binds in a positively charged groove flanked in its central segment by 303 and 764, and by 745 and 153 at its downstream and upstream edges, respectively.

Conjugates 385, 388, 393, 394, and 644 cleave RNA in EC24 ~5 nt away from the 3′ end (Figure 4A, lanes 13–22). This is consistent with simple extension of the 3 bp RNA:DNA duplex in ITC3, as well as with structure-function studies, indicating that in the ITC, 393 and 394 are near the RNA ~5 nt away from the 3′ end (Brieba et al., 2001).

In ITC7, 239, 385, 388, and 644 also cleave RNA ~5 nt away from the 3′ end (Figure 4B; failure to detect cleavage by 393 and 394 may be due to the fact that mutation of 393/394 increases RNA dissociation from the ITC). Since this is similar to the positions of RNA cleavage by 385, 388, and 644 in EC24, its suggests that the position of the RNA:DNA hybrid in the transcription complex does not change markedly upon transition to elongation. However, cleavage by 385/388 intensifies in the EC, especially for 385 (Figure 4A, lanes 14 and 15), similar to the increase in 385/388 T strand cleavage upon formation of EC13 (Figure 2B, lanes 4, 5, 9, and 10). Cleavage by 239 is strong in ITC7 (Figure 4B, lane 2), but is undetectable in the EC (not shown), paralleling the disappearance of 239 cleavage of T strand within the transcription bubble upon transition to elongation (Figure 2B, lanes 4 and 5).

Finally, note that 385, 388, 393, 394, and 239 in Figures 2 and 3 do not cleave the T strand region expected to hybridize with RNA. If this reflects protection by RNA, these same conjugates should cleave the RNA complementary to the protected T strand regions. This is confirmed by the RNA cleavage data. For example, 239 does not cleave T strand downstream of +1 in ITC7 (Figure 3A, lanes 3–7), but does cleave RNA opposite +1 to +4 of the T strand (Figure 4A, lane 2), a cleavage pattern consistent with the location of the RNA in ITC3 (Figure 3B).

AFM Indicates a Similar DNA Bend Angle in the EC and ITC

Cleavage of downstream (+20) DNA in EC13 by upstream conjugates (Figures 2F and 2G) was unexpected. This could mean that DNA in the EC is bent more than 90° so that DNA downstream of the RNA would approach the upstream face of the polymerase. To assess this we used atomic force microscopy. Without polymerase, 0.3 kb DNA molecules containing a T7 promoter 0.1 kb from one end were either straight or smoothly bent over a shallow angle (Figure 5A). ITCs with a 6 nt RNA (Figure 5B) or ECs with a 13 nt RNA (Figure 5C) were formed with this DNA and imaged in air. Sixty particles, chosen from fields of either ITCs or ECs, based on the apparent presence of a polymerase ~0.03 μM from one end of the DNA, had an average bend of 55° ± 20° for ECs and 59° ± 30° for ITCs. The bends in ECs and ITCs are therefore similar and within the 40°–60° range previously estimated for the bend in a T7RNAP open complex (Ujvari and Martin, 2000).

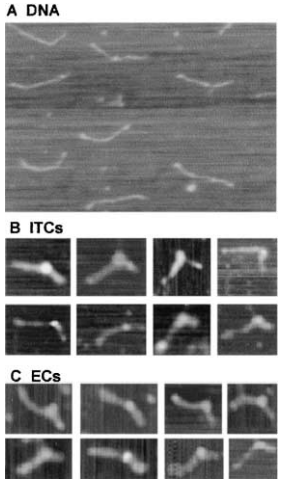

Figure 5. AFM of Transcription Complexes

(A) AFM image of 304 bp DNA molecules containing a T7 promoter 98 bp from one end.

(B) Images of ITCs with 6 nt RNAs formed with DNA from (A).

(C) Images of ECs with 13 nt RNAs formed with this same DNA.

Discussion

The cleavage patterns seen as T7RNAP initiates transcription are summarized in Figure 6. As RNA grows from 1 to 7 nt, cleavages upstream of −4 do not shift (Figure 6, Static), indicating that interactions with these regions anchor the polymerase even as more downstream DNA threads through the complex. An exception is T strand cleavage by thumb residues 385/388, which shifts from −9 to −2 when the RNA is extended from 4 to 6 nt, and NT strand cleavage at −5 by 385/388, which decreases markedly at the same point. Since similar changes are not seen for other conjugates that cleave upstream of −4, the changes in 385/388 cleavage are most simply explained as due to bending of the thumb. A similar change is seen in the thumb of DNAP I (KF) upon binding primer-template (Beese et al., 1993).

While cleavages upstream of −4 are static during initial transcription, cleavage sites downstream of +5 (due to 239 and 745) shift downstream as the RNA is extended (Figure 6, Moving). T strand cleavage by 394 and 239 in the region between the upstream edge of the transcription bubble (−5) and the RNA also changes as the RNA is extended from 1 to 7 nt (Figure 6, Scrunching). However, unlike cleavages downstream of the RNA, cleavage patterns in this region do not simply shift downstream, but lengthen by downstream extension, consistent with the idea that the T strand in this region scrunches into the transcription complex as the RNA is extended (Cheetham and Steitz, 1999; Brieba and Sousa, 2001a).

The −1 and −3 bp in a T7RNAP ITC remain open as RNA is extended from 1 to 7 nt (Place et al., 1999;

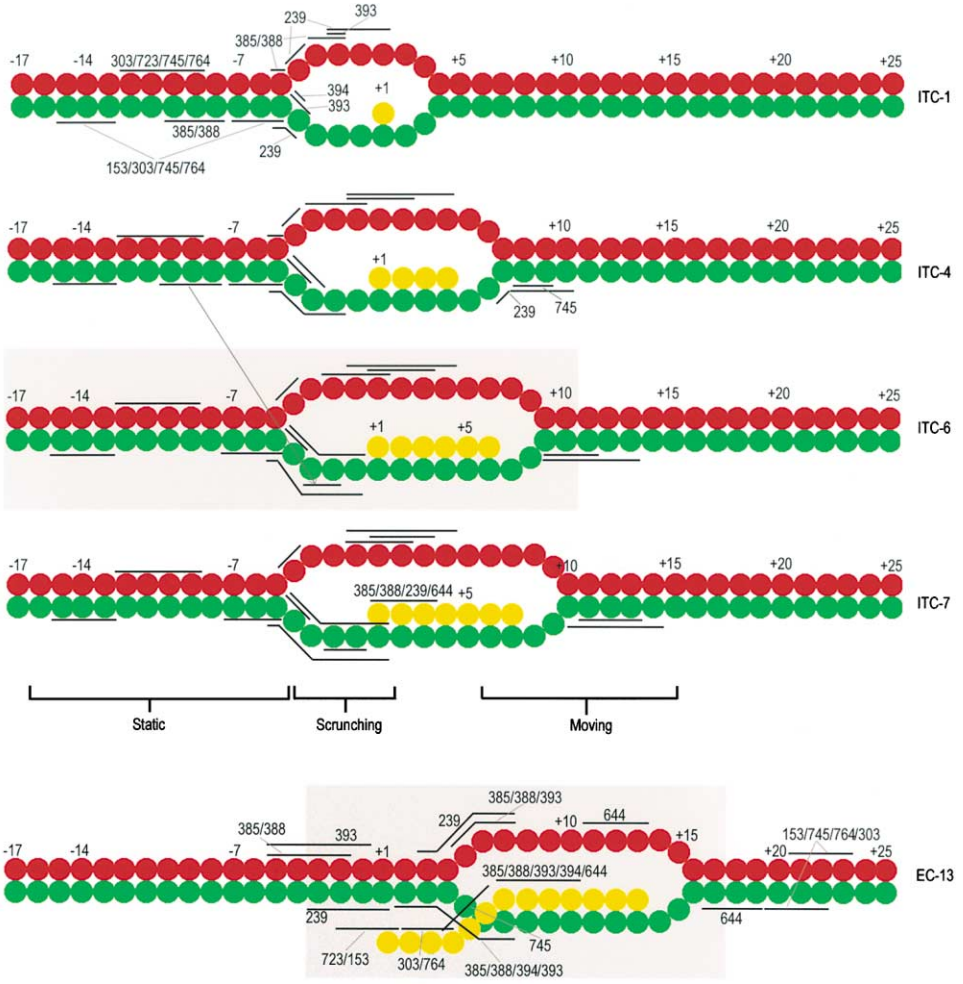

Figure 6. Summary of Cleavage Patterns

NT, T, and RNA are in red, green, and yellow, respectively. Cleavage ranges are indicated by horizontal bars and are stacked identically in ITCs 1–7, but are labeled explicitly (by conjugate number) only in ITCs1, 4, and 7, as well as in EC13. Gray boxes in ITC6 and EC13 indicate extent of RNAP footprint in those complexes (Ikeda and Richardson, 1986).

Brieba and Sousa, 2001a, 2001b) and as the size of the unwound region grows (Villemain et al., 1997). The transcription bubble closes 1–2 nt downstream of the RNA 3′ end (Huang and Sousa, 2000). The length of unpaired NT strand must therefore grow as the RNA is extended from 1 to 7 nt, as shown in Figure 6. However, this does not lead to translocation of the NT strand, at least not relative to 239 and 393, which cleave at similar positions on the NT strand as the RNA is extended from 1 to 7 nt (changes in NT strand cleavage upon RNA extension from 1 to 4 nt may reflect stabilization of the open complex). A shift in the center of NT strand cleavage by 385/388 from −2 to +1 as the RNA is extended from 4 to 7 nt may reflect bending of the thumb (rather than NT strand translocation) because such a bend would move 385/388 downstream along the NT strand, and because the other conjugates that cleave in this region do not show similar shifts in their cleavage sites.

RNA extension from 7 to 13 nt results in several changes in cleavage patterns, some of which can be attributed to translocation, but many of which may not (Figure 6, EC13). Among the latter are the increases in T strand and RNA cleavage by 385/388, T and NT strand cleavage by 644 in EC13 (which does not cleave DNA in the ITC), and appearance of NT strand cleavage by 385, 388, and 393 upstream of the transcription bubble (between −1 and −5) in the EC. Changes in cleavage patterns due to conformational changes (rather than translocation or DNA rearrangement) were assigned to instances where the cleavage positions of a conjugate changed in a manner distinct from those of other conjugates that cleaved in the same regions. This is suggested for 239, which—like 385, 388, or 394—cleaves T strand within the transcription bubble in ITC7, and which—like 385, 388, and 644—also cleaves RNA in ITC7 (Figure 6). In EC13, 385, 388, and 394 continue to cleave the T strand at positions (relative to the RNA 3′ end) similar to those seen in ITC7, and 385, 388, and 644 cleave RNA in the EC as they do in the ITC. However, in EC13, 239 cleaves neither the RNA nor the T strand within the transcription bubble, and T strand cleavage is, instead, directed upstream of the bubble, suggesting

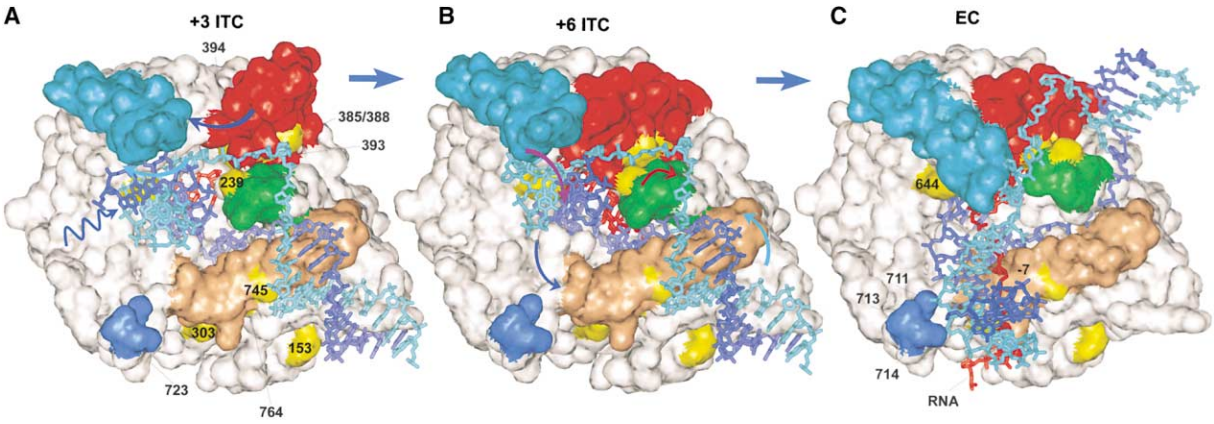

Figure 7. Structural Transitions during Transcription Initiation by T7 RNAP

(A) Structure of ITC3 with modeled T strand from +6 to +16 and NT strand from −3 to +16. The thumb (aa 330–410; red), intercalating hairpin (aa 232–242; green), promoter recognition loop (aa 740–770; brown), fingers flap (aa 586–620; cyan), positively charged cluster (K711/713/714; blue), and positions of Fe-BABE conjugation (yellow) are highlighted. RNA is red, T strand is blue, and NT strand is cyan.

(B) Modeled structure of ITC6.

(C) Model of an EC. Arrows indicate movements in DNA and protein accompanying progression through the initiation reaction. See text for details.

that 239 participates in a conformational change upon transition to elongation. The most dramatic change upon transition to elongation is loss of cleavage by the upstream conjugates (153, 303, 723, 745, 764) in the region upstream of the transcription bubble and simultaneous appearance of cleavage downstream of the bubble. Because this change involves all of the upstream conjugates, including those on the promoter recognition loop (745, 764) and N-terminal domain (153, 303), it is unlikely to be due to a conformational change in the polymerase (though this cannot be ruled out), and may instead reflect a change in how DNA is bound within the complex.

Figure 7 models a set of structural transitions that can account for the changes in cleavage patterns. The starting point is the ITC3 crystal structure with NT strand downstream of −4 and T strand downstream of +5 modeled in, based both on constraints imposed by the cleavage patterns and data on the size of the melted region in the ITC (Figure 7A). As the RNA is extended from 3 to 6 nt, the T strand scrunches into the complex (suggested by the wavy blue arrow in Figure 7A), and more NT strand becomes unpaired and loops out (cyan arrow in Figure 7A) but does not translocate across the polymerase. The thumb also bends in, toward the RNA and the template binding cleft (indicated by the dark blue arrow), hinging between 388 and 393.

When the EC forms, additional transitions occur. Residue 239 turns away from the T strand binding cleft and downstream DNA, and toward DNA upstream of the transcription bubble. As suggested by the red arrow in Figure 7B, this could involve rotation of the intercalating hairpin by ~90°. Increased T strand and RNA cleavage by 385/388 upon transition to elongation might be due to a conformational change that limits diffusion of OH· out of the cleft. For example, movement of the fingers "flap" (in cyan in Figure 7), as suggested by the purple arrow in Figure 7B, could help trap OH· generated at 385/388 near the T strand and RNA, leading to increased cleavage.

To account for differences between the DNA cleavage patterns of upstream conjugates (153, 303, 723, 745, and 764) in the ITCs versus EC13, we suggest that upon transition to elongation, DNA downstream of the transcription bubble bends toward the promoter recognition loop (suggested by the blue arrow in Figure 7B), while DNA upstream of the bubble bends away from the loop (as suggested by the cyan arrow). This would maintain a similar DNA bend angle in the ITC and EC, as suggested by AFM, but would cause loss of cleavage of the upstream DNA by the upstream conjugates and appearance of cleavage downstream of the RNA. It would also explain the appearance of cleavage by 385, 388, and 393 in NT strand upstream of the transcription bubble, since movement of the upstream DNA away from the promoter recognition loop would place this region of the NT strand nearer to these residues (Figure 7C).

Like the bending of the thumb, placement of the upstream DNA as shown in Figure 7C has precedent in a DNAP I (KF) primer-template structure. In that structure (Beese et al., 1993), primer-template binds in a cleft beneath the thumb that, in T7RNAP, is partially occupied by the intercalating hairpin. Thus, the upstream DNA in the T7RNAP and DNAP I ECs may bind similarly, the major difference being that the former has an intercalating hairpin that forces DNA in this region to bind in unwound form (Figure 7C).

In the EC13 used here, the RNA:DNA hybrid is, at most, 7 bp (Brieba and Sousa, 2001b). In Figure 7C, a 7 bp hybrid is modeled and −8 to −13 of the RNA is placed in the positively charged groove identified in Figure 4C. This constrains RNA from −7 to −9 to pass over the promoter recognition loop as indicated by the labeled −7 nt in Figure 7C. This agrees with observations that RNA 8 nt from the 3′ end crosslinks near 745 on the recognition loop (Temiakov et al., 2000).

The proposed structural transitions appear to be functionally concerted. Bending of the thumb may make room for the new position of the upstream DNA in the

EC, and both bending of the thumb and rotation of the intercalating hairpin may make room for a 7–8 bp hybrid in the T strand binding cleft, which has otherwise been proposed to be constrained to ~3 bp due to clashes with the thumb and hairpin (Cheetham and Steitz, 1999). Bending of the thumb may be driven by RNA:thumb contacts since the RNA appears to contact the thumb when it reaches ~5 nt in length (Brieba et al., 2001). Movement of the fingers' flap may help bend downstream DNA toward the promoter recognition loop. The conformational changes in the thumb and fingers may stabilize the EC. Strikingly, bending of the downstream DNA causes it to approach a cluster of positively charged residues (K711/713/714, Figure 7C), which may help orient the downstream DNA in the EC. Movement of the upstream DNA away from the promoter recognition loop may be a consequence and/or a cause of promoter release, and may be important in keeping the elongating enzyme from sticking to promoter-like sequences. T7 RNAP is inhibited by T7 lysozyme, which causes a change in polymerase conformation (Jeruzalmi and Steitz, 1998; Huang et al., 1999), including a change in the putative RNA binding groove. T7RNAP becomes resistant to T7 lysozyme upon transition to elongation (Zhang and Studier, 1997), so it is possible that the RNA binding in this groove inhibits the conformational change caused by lysozyme binding.

Other interpretations for the cleavage patterns seen here could be offered. However, our models are constrained by biochemical and crystallographic data, and we have proposed a minimal set of reasonable structural changes that can account for our cleavage data. Apparent conformational changes were limited to structures (thumb, fingers, intercalating hairpin) known to be mobile by crystallography. Examination of cleavage in the T and NT strands and RNA by a large number of conjugates provided crossvalidation. Thus, a discontinuous change in T strand cleavage by 388 upon RNA extension from 4 to 6 nt coincided with an analogous change in the NT strand and was reinforced by observation of similar changes with the adjacent 385 conjugate. Interpretation was assisted by the high resolution of cleavage. For example, though 385 and 388 are directly adjacent on thumb helix N, the cleavage patterns of these conjugates are clearly distinct, and in Figure 3 we distinguish translocation of the T strand by, at most, 1 nt.

Investigators attempting to understand macromolecular machinery increasingly confront situations where direct structural data is limited to a small number of incomplete and irregularly spaced snapshots, but where processes are likely to be continuously dynamic. Cleavage by tethered chemical reagents can fill in the gaps in such processes and is complementary to energy transfer approaches. In particular, structural changes that may not involve movement across large distances, but that mask or unmask cleavage sites (as seen when the thumb bends), may be easier to detect with a chemical probe. Though our study was facilitated by the fact that intermediates in transcription initiation can be prepared by NTP limitation, quench-flow approaches would allow application of this method to probe the conformational dynamics of other macromolecular machines. Realistic movies of such machinery in action, replete with the concerted structural transitions seen here for a transcription initiation reaction, should emerge.

Experimental Procedures

Mutant Enzyme Preparation and Conjugation

Mutants were prepared as described (Brieba et al., 2001) and stored in 20 mM Tris-HCl (pH 8.0), 0.5 M NaCl, 5 mM DTT, 1 mM EDTA, 50% glycerol (storage buffer). Before conjugation, enzymes were exchanged into 20 mM Tris-HCl (pH 8.0), 0.5 M NaCl, 1 mM EDTA, 50% glycerol by gel filtration and diluted to 10 μM. Fe-BABE was added to 0.5 mM and incubated for 1 hr at 37°C. Unreacted Fe-BABE was removed by gel filtration, and the conjugated enzyme was stored in storage buffer (with 1 mM DTT) at −70°C. The percent conjugation was determined from DTNB reactivity before and after conjugation.

Cleavage Reactions

A synthetic template 42 bp in length with a consensus −17 to +6 T7 promoter and a T strand sequence from +7 to +25 of GGC CTTAAGCTCGAGCGGG was labeled at the 5′ end of either the T or NT strand. DNA and RNAPs were mixed at 0.1 and 0.3 μM, respectively, in 10 mM Tris-HCl (pH 8.0), 10 mM NaCl, 6 mM $MgCl_2$, 5 mM DTT, 2 mM spermidine (transcription buffer). NTPs were added to 0.5 mM and reactions were incubated for 3 min at 37°C. Reactions were split in two, and ascorbic acid and H_2O_2 were added to 1 aliquot to 10 and 25 mM, respectively. After 2 min, reactions were quenched and an equal volume of 95% formamide, 20 mM EDTA, 0.01% xylene cyanol was added. Reactions were placed in boiling water for 5 min, placed on ice, and resolved by electrophoresis on 17.5% polyacrylamide, 0.8% bis-acrylamide, 7 M urea gels in TBE. RNA cleavage in the ITC used supercoiled pT7-7 (Brieba and Sousa, 2001b), whose initially transcribed sequence (ITS) is GGGAGCUU, as template. RNAP and template were mixed in transcription buffer and incubated for 10 min at RT, followed by addition of GTP and ATP and a further 3 min incubation. Reactions were placed on ice for 2 min, followed by addition of 3′-dUTP and [α-^{32}P]CTP. The reaction was split in two. Ascorbic acid and H_2O_2 were added to one aliquot, reactions were placed at 37°C for 1 min, quenched, mixed with formamide loading buffer, and resolved on 20% polyacrylamide, 1% bis-acrylamide, 6 M urea gels. RNA cleavage in the EC used BglI-II linearized pPK7 (RNA seq.: GAGGGAGGGAGGGAGGGAGACU; Mentesanas et al., 2000). Template and RNAP in transcription buffer were incubated at RT for 20 min; GTP, ATP, [α-^{32}P]CTP, and 3′-dUTP were added and reactions were incubated for 4 min at 37°C. Reactions were split in two, and one aliquot was reacted with ascorbate and H_2O_2 for 2 min at 37°C, quenched, and resolved as described above. Reactions were also done with heparin added to 0.1 mg/ml after NTP addition. Gels were analyzed with a Molecular Dynamics Phosphorimager.

Atomic Force Microscopy

pT7-5 (Tabor and Richardson, 1985) was digested with Fok I to release a 304 bp fragment containing a T7 promoter 98 bp from one end. Gel-purified fragment was mixed at 10^{-8} M with 10^{-8} M RNAP in transcription buffer with either 0.5 mM GTP and ATP (ITCs), or 0.5 mM GTP, ATP, CTP, and 3′-dUTP (ECs). Reactions were incubated 15 min at 37°C and diluted 1:10 with transcription buffer, and then 3 μl was pipetted onto freshly cleaved ruby mica. After 2 min, the mica was rinsed with water, dried in a nitrogen stream, and imaged in air.

Acknowledgments

Supported by NIH Grant GM52522 and the Welch Foundation. We thank Pawel Osmulski and Maria Gaczynska for assistance with AFM.

Received: April 16, 2002
Revised: June 3, 2002

References

Beese, L.S., Derbyshire, V., and Steitz, T.A. (1993). Structure of DNA polymerase I Klenow fragment bound to duplex DNA. Science *260*, 352–355.

Brieba, L.G., and Sousa, R. (2001a). T7 promoter release mediated by DNA scrunching. EMBO J. *20*, 6826–6835.

Brieba, L.G., and Sousa, R. (2001b). The T7 RNA polymerase intercalating hairpin is important for promoter opening during initiation but not for RNA displacement or transcription bubble stability during elongation. Biochemistry *40*, 3882–3890.

Brieba, L.G., Gopal, V., and Sousa, R. (2001). Scanning mutagenesis reveals roles for helix n of the bacteriophage T7 RNA polymerase thumb subdomain in transcription complex stability, pausing, and termination. J. Biol. Chem. *276*, 10306–10313.

Carpousis, A.J., and Gralla, J.D. (1980). Cycling of ribonucleic acid polymerase to produce oligonucleotides during initiation *in vitro* at the *lac* UV5 promoter. Biochemistry *19*, 3245–3253.

Cheetham, G., and Steitz, T.A. (1999). Structure of a transcribing T7 RNA polymerase initiation complex. Science *286*, 2305–2309.

Cheetham, G.M., Jeruzalmi, D., and Steitz, T.A. (1999). Structural basis for initiation of transcription from an RNA polymerase-promoter complex. Nature *399*, 80–83.

Cramer, P., Bushnell, D.A., and Kornberg, R.D. (2001). Structural basis of transcription: RNA polymerase II at 2.8 angstrom resolution. Science *292*, 1863–1876.

Greiner, D.P., Miyake, R., Moran, J.K., Jones, A.D., Negishi, T., Ishihama, A., and Meares, C.F. (1997). Synthesis of the protein cutting reagent iron (S)-1-(p-bromoacetamidobenzyl)ethylenediamine-tetraacetate and conjugation to cysteine side chains. Bioconjug. Chem. *8*, 44–48.

Gruber, T.M., Markov, D., Sharp, M.M., Young, B.A., Lu, C.Z., Zhong, H.J., Artsimovitch, I., Geszvain, K.M., Arthur, T.M., Burgess, R.R., et al. (2001). Binding of the initiation factor sigma(70) to core RNA polymerase is a multistep process. Mol. Cell *8*, 21–31.

Han, H., and Dervan, P.B. (1994). Visualization of RNA tertiary structure by RNA-EDTA-Fe(II) autocleavage: Analysis of tRNAPhe with uridine-EDTA-Fe(II) at position 47. Proc. Natl. Acad. Sci. USA *91*, 4955–4959.

Hansen, U.M., and McClure, W.R. (1980). Role of sigma subunit of *Escherichia coli* RNA polymerase initiation. II. Release of sigma from ternary complexes. J. Biol. Chem. *255*, 9564–9570.

Huang, J., and Sousa, R. (2000). T7 RNA polymerase elongation complex structure and movement. J. Mol. Biol. *303*, 347–358.

Huang, J., Villemain, J., Padilla, R., and Sousa, R. (1999). Mechanisms by which T7 lysozyme specifically regulates T7 RNA polymerase during different phases of transcription. J. Mol. Biol. *293*, 457–475.

Ikeda, R.A., and Richardson, C.C. (1986). Interactions of the RNA polymerase of bacteriophage T7 with its promoter during binding and initiation of transcription. Proc. Natl. Acad. Sci. USA *83*, 3614–3618.

Jia, Y., and Patel, S.S. (1997). Kinetic mechanism of transcription initiation by bacteriophage T7 RNA polymerase. Biochemistry *36*, 4223–4232.

Jeruzalmi, D., and Steitz, T.A. (1998). Structure of T7 RNA polymerase complexed to the transcriptional inhibitor T7 lysozyme. EMBO J. *17*, 4101–4113.

Krummel, B., and Chamberlin, M. (1989). RNA chain initiation by *Escherichia coli* RNA polymerase. Structural transitions of the enzyme in early ternary complexes. Biochemistry *28*, 7829–7842.

Kuznedelov, K., Minakhin, L., Niedziela-Majka, A., Dove, S.L., Rogulja, D., Nickels, B.E., Hochschild, A., Heyduk, T., and Severinov, K. (2002). A role for interaction of the RNA polymerase flap domain with the σ subunit in promoter recognition. Science *295*, 855–857.

Landick, R. (2001). RNA polymerase clamps down. Cell *105*, 567–570.

MacDonald, L.E., Zhou, Y., and McAllister, W.T. (1993). Termination and slippage by bacteriophage T7 RNA polymerase. J. Mol. Biol. *232*, 1030–1047.

MacDonald, L.E., Durbin, R.K., Dunn, J.J., and McAllister, W.T. (1994). Characterization of two types of termination signals for bacteriophage T7 RNA polymerase. J. Mol. Biol. *238*, 145–158.

Martin, C.T., Muller, D.K., and Coleman, J.E. (1988). Processivity in early stages of transcription by T7 RNA polymerase. Biochemistry *27*, 3966–3974.

Mekler, V., Kortkhonjia, E., Mukhopadhyay, J., Knight, J., Revyakin, A., Kapanidis, A.N., Niu, W., Ebright, Y.W., Levy, R., and Ebright, R.H. (2002). Structural organization of bacterial RNA polymerase holoenzyme and the RNA polymerase-promoter open complex. Cell *108*, 599–614.

Mentesanas, P.E., Chin-Bow, S.T., Sousa, R., and McAllister, W.T. (2000). Characterization of bacteriophage T7 RNA polymerase elongation complexes. J. Mol. Biol. *302*, 1049–1062.

Mukhopadhyay, J., Kapanidis, A.N., Mekler, V., Kortkhonjia, E., Ebright, Y.W., and Ebright, R.H. (2001). Translocation of 70 with RNA polymerase during transcription: fluorescence resonance energy transfer assay for movement relative to DNA. Cell *106*, 453–463.

Nudler, E. (1999). Transcription elongation: structural basis and mechanisms. J. Mol. Biol. *288*, 1–12.

Palangat, M., and Landick, R. (2001). Roles of RNA:DNA hybrid stability, RNA structure, and active site conformation in pausing by human RNA polymerase II. J. Mol. Biol. *311*, 265–282.

Place, C., Oddos, J., Buc, H., McAllister, W.T., and Buckle, M. (1999). Studies of contacts between T7 RNA polymerase and its promoter reveals features in common with multisubunit RNA polymerases. Biochemistry *38*, 4948–4957.

Sousa, R., Patra, D., and Lafer, E.M. (1992). Model for the mechanism of bacteriophage T7 RNAP transcription initiation and termination. J. Mol. Biol. *224*, 319–334.

Sousa, R., Chung, Y.J., Rose, J.P., and Wang, B.C. (1993). Crystal structure of bacteriophage T7 RNA polymerase at 3.3 Å resolution. Nature *364*, 593–599.

Sousa, R., Rose, J., and Wang, B.C. (1994). The thumb's knuckle. Flexibility in the thumb subdomain of T7 RNA polymerase is revealed by the structure of a chimeric T7/T3 RNA polymerase. J. Mol. Biol. *244*, 6–12.

Straney, D.C., and Crothers, D.M. (1987). A stressed intermediate in the formation of stability initiated RNA chains at the *Escherichia coli lac* UV5 promoter. J. Mol. Biol. *193*, 267–278.

Tabor, S., and Richardson, C.C. (1985). A bacteriophage T7 RNA polymerase/promoter system for controlled exclusive expression of specific genes. Proc. Natl. Acad. Sci. USA *82*, 1074–1078.

Temiakov, D., Mentesanas, P.E., Ma, K., Mustaev, A., Borukhov, S., and McAllister, W.T. (2000). The specificity loop of T7 RNA polymerase interacts first with the promoter and then with the elongating transcript, suggesting a mechanism for promoter clearance. Proc. Natl. Acad. Sci. USA *97*, 14109–14114.

Uptain, S.M., Kane, C.M., and Chamberlin, M.J. (1997). Basic mechanisms of transcript elongation and its regulation. Annu. Rev. Biochem. *66*, 117–172.

Ujvari, A., and Martin, C.T. (2000). Evidence for DNA bending at the T7 RNA polymerase promoter. J. Mol. Biol. *295*, 1173–1184.

Villemain, J., and Sousa, R. (1998). Specificity in transcriptional regulation in the absence of specific DNA binding sites: the case of T7 lysozyme. J. Mol. Biol. *281*, 793–802.

Villemain, J., Guajardo, R., and Sousa, R. (1997). Role of open complex instability in kinetic promoter selection by bacteriophage T7 RNA polymerase. J. Mol. Biol. *373*, 958–977.

Zhang, X., and Studier, F.W. (1997). Mechanism of inhibition of bacteriophage T7 RNA polymerase by T7 lysozyme. J. Mol. Biol. *269*, 10–27.

Zhang, G., Campbell, E.A., Minakhin, L., Richter, C., Severinov, K., and Darst, S.A. (1999). Crystal structure of *Thermus aquaticus* core RNA polymerase at 3.3 Å resolution. Cell *98*, 811–824.